# Diverse innate immune factors protect yeast from lethal viral pathogenesis

Sabrina Chau[1], Jie Gao[1], Annette Diao[1], Michelle Cao[1], Alan R. Davidson[1,2], and Marc D. Meneghini[1*]
[1]Department of Molecular Genetics, University of Toronto, 661 University Ave, Toronto, ON, M5G 1M1, Canada.
[2]Department of Biochemistry, University of Toronto, 661 University Ave, Toronto, ON, M5G 1M1, Canada.

[*]Corresponding Author

**Although the budding yeast *Saccharomyces cerevisiae* is chronically infected with a double-stranded RNA virus called L-A, the lack of any known L-A fitness consequence has hindered use of this model organism for the study of host-virus interactions. Here we show that L-A causes lethal pathogenesis in cells lacking parallel-acting viral attenuation pathways. Leveraging this discovery, we identify known and new antiviral factors exploiting unbiased genetic screens and determine that rampant L-A proliferation causes proteostatic stress.**

In recent years, newly characterized antiviral systems have been found to be remarkably conserved from bacteria to mammals, revealing the potential to gain unique insight into these systems through the study of microbial organisms[1]. Despite the enthusiasm generated by these findings, the key microbial model organism *Saccharomyces cerevisiae* (budding yeast) has been minimally exploited for studies of viral defense, primarily because it is not infected with exogenously transmitted viruses. However, most yeast strains are infected with an endogenous double stranded RNA (dsRNA) virus called L-A, and previous studies have identified conserved antiviral systems that attenuate L-A replication[2]. Although these systems do not lead to eradication of L-A, we show here that they prevent massive over-proliferation of L-A that leads to proteostatic stress and lethality. Exploiting this new insight, we asked if the powerful genetic screening methods available in yeast could be used to identify additional conserved antiviral systems. Validating this approach, we discovered antiviral functions for the yeast homologs of polyA-binding protein (PABPC1) and the La-domain containing protein Larp1, which are both involved in viral innate immunity in humans[3,4]. We also identify new antiviral functions for the RNA exonucleases *REX2* and *MYG1*, both of which have distinct but poorly characterized human and bacterial homologs. These findings highlight the potential of yeast as a powerful model system for studies of the ubiquitous host-virus arms race.

34 L-A belongs to the broadly dispersed *Totiviridae* family of double stranded RNA (dsRNA)
35 viruses, which has no extracellular phase and is transmitted vertically through cell division or fusion[2]. L-
36 A transcripts encode the capsid (Gag) proteins that comprise most of its viral particle as well as a Gag-
37 pol fusion protein produced at much lower levels that provides RNA dependent RNA polymerase
38 activity responsible for replication and transcription. Encapsidation of viral transcripts within nascent
39 particles completes the L-A lifecycle[2]. L-A replication is maintained at a low level through the activities
40 of the *SKI2*, *3*, and *8* genes, which encode subunits of a conserved ribosome-associated complex that
41 opposes the translation of transcripts such as those encoded by L-A that lack polyA tails[5-7]. A separate
42 pathway of L-A attenuation is provided by Xrn1, a 5'-3' exoribonuclease that degrades uncapped
43 mRNAs[8,9]. Both of these systems have been associated with anti-viral defense in mammals[10-13].
44 We showed previously that L-A replication was held in check during sporulation by the
45 mitochondrial DNA/RNA endonuclease Nuc1, a homolog of endonuclease G (EndoG) found in all
46 eukaryotes and many prokaryotes[14]. EndoG is involved in mammalian programmed cell death that
47 frequently occurs in virus infected cells, and programmed cell death is intrinsic to yeast sporulation[15-18].
48 These and other observations have led to speculation that Nuc1/EndoG may reflect a prokaryotic
49 antiviral origin of programmed cell death[19]. To query *NUC1* anti-viral function outside of sporulation
50 and its associated programmed cell death, we investigated L-A attenuation in mitotic haploid cells in the
51 reference BY4742 strain background. Visualization of L-A dsRNA using ethidium bromide staining of
52 electrophoresed RNA revealed that while *nuc1*Δ and *ski3*Δ single mutants exhibited no effect,
53 combining *nuc1*Δ and *ski3*Δ led to a large increase in L-A dsRNA **(Fig 1A)**. We corroborated these
54 findings using immunofluorescence microscopy with a dsRNA antibody widely used to detect
55 replicating RNA viruses[20,21]. These images revealed L-A dsRNA to accumulate in foci, reminiscent of
56 "viral factory" sites of viral replication observed in human cells **(Fig 1B and S1)**[22]. Consistent with
57 previous findings in other strain backgrounds, western blotting showed that Gag protein levels were
58 elevated in *nuc1*Δ and *ski3*Δ mutants[8,14,23], and we determined that *nuc1*Δ *ski3*Δ double mutants
59 accumulated massively elevated Gag levels, confirming that *NUC1* and *SKI3* participate in separate
60 antiviral pathways **(Fig 1C)**.
61 We used spot test growth assays to determine if high L-A viral load had any fitness consequence
62 and found that *nuc1*Δ *ski3*Δ double mutants grew normally at 30˚ C but exhibited conditional lethality at
63 37˚ C **(Fig 1D)**. Modest growth defects of *nuc1*Δ and *ski3*Δ single mutants were observed at high
64 temperature when cells were grown with glycerol rather than glucose as the carbon source, a condition
65 under which yeast relies on mitochondrial respiration **(Fig 1D)**. These growth phenotypes were
66 completely reversed in isogenic strains cured of L-A (L-A$^0$), implying that unrestricted L-A replication

67 caused them (**Fig 1D**).

68 As expected, a *NUC1*-expressing plasmid restored viability to a *nuc1*Δ *ski3*Δ strain grown at high
69 temperature and elicited a corresponding decrease in Gag levels (**Fig 1C and 1D**). We observed similar
70 suppression of *nuc1*Δ *ski3*Δ using plasmid driven *XRN1* over-expression, suggesting that Xrn1 repressed
71 L-A via a parallel mechanism **(Fig 1C and 1D)**. Consistent with this model, *nuc1*Δ *xrn1*Δ mutants
72 accumulated greatly elevated levels of Gag and exhibited L-A-dependent conditional lethality at high
73 temperature **(Fig S2)**, and *xrn1*Δ *ski3*Δ mutants are inviable[24]. We conclude that Nuc1, Ski3 and Xrn1
74 convergently oppose L-A, and that L-A causes lethal pathogenesis at high temperature when
75 unattenuated **(Fig 1E)**.

76 Since *XRN1* over-expression suppressed the growth defects of a *nuc1*Δ *ski3*Δ strain, we
77 hypothesized that over-expression of other antiviral factors would produce a similar effect, and that this
78 phenomenon could be used as a screen to identify new antiviral systems. To test this idea, we employed
79 a high-copy plasmid suppression screen to detect genes whose overexpression alleviated the conditional
80 lethality of *nuc1Δ ski3Δ*. Using this strategy, we identified *SRO9*, *SLF1*, and *PAB1* as high-copy
81 suppressors, all of which encode ribosome-associated RNA binding proteins **(Fig 2A)**[25,26]. Sro9 and Slf1
82 are paralogous lupus-autoantigen (La) domain containing proteins broadly found in eukaryotes.
83 Interestingly, the human Sro9/Slf1 ortholog Larp1 was recently found to bind to SARS-Cov-2 plus-
84 strand ssRNA and to oppose its replication in human cells through an unknown mechanism[3]. *PAB1*
85 encodes the highly conserved PolyA-Binding Protein (PABPC1 in humans), which is a common target
86 of viral inhibition through diverse mechanisms[4]. *PAB1* and *SRO9* overexpression markedly reduced Gag
87 levels, explaining their rescuing phenotypes **(Fig 2B)**. Curiously, even though *SLF1* overexpression
88 rescued the *nuc1*Δ *ski3*Δ growth defect just as well as *SRO9*, it did not lead to any reduction in Gag
89 levels **(Fig 2A and 2B)**. These findings suggest that *SRO9* rescues cells by opposing L-A replication and
90 that *SLF1* protects cells from the pathogenic consequences of elevated viral replication **(Fig 1E)**.

91 To gain insight into the divergent mechanisms of Sro9 and Slf1, we considered further what
92 physiological consequences L-A pathogenesis has and how *SRO9*/*SLF1* might differentially impact
93 them. We noted a previous study in which deletions of *NUC1* or of *SKI*-complex genes led to weak
94 induction of a proteostatic stress GFP reporter gene controlled by Hsf1, a conserved transcription factor
95 that senses proteostatic stress and activates the gene expression response[27-30]. Using flow cytometry with
96 this reporter (HSE-GFP), we determined that a *nuc1*Δ *ski3*Δ double mutant exhibited strong activation of
97 HSE-GFP and that this activation was reverted in L-A$^0$ strains **(Fig 2C and S3)**. We hypothesized that
98 the massive accumulation of Gag observed in *nuc1*Δ *ski3*Δ mutants accounted for this proteostatic stress
99 response. Supporting this, HSE-GFP activation of a *nuc1*Δ *ski3*Δ double mutant was reverted by *PAB1*

100 or *SRO9* over-expression, but not by *SLF1* over-expression, mirroring these genes respective
101 consequences for Gag accumulation **(Fig 2B and 2C)**. The evolutionary divergence of *SRO9* and *SLF1*
102 has thus resulted in different viral-protective mechanisms, with *SRO9* opposing viral protein
103 accumulation and associated proteostatic stress, and *SLF1* possibly protecting cells from the toxic
104 consequences of viral induced proteostatic stress **(Fig 1E)**.
105 To identify new antiviral factors using a different approach, we searched a curated genetic
106 interaction database for gene deletions that caused a synergistic growth defect when combined with
107 *nuc1Δ* in at least two high-throughput screening studies. We found fifteen such examples[31], two of
108 which we confirmed as new viral attenuation factors. The first of these, *REX2*, is conserved from
109 bacteria to humans[32]. Both Rex2 and its human homolog REXO2 are mitochondrial-localized 3'-5'
110 RNA exonucleases that contain an EXOIII domain widely found in prokaryotic and eukaryotic proteins,
111 including the interferon stimulated antiviral protein ISG20[33-37]. Mutant strains combining *rex2*Δ with
112 *nuc1*Δ accumulated greatly increased levels of Gag and exhibited L-A-dependent lethality at high
113 temperature **(Fig 2D and 2E)**. Remarkably, *nuc1*Δ *ski3*Δ *rex2*Δ and *nuc1*Δ *xrn1*Δ *rex2*Δ triple mutants
114 were inviable under all growth conditions and these defects were reversed in L-A$^0$ strains **(Fig S4)**.
115 These findings demonstrate the severe pathogenic potential of L-A and identify a new and highly
116 conserved mitochondrial localized antiviral RNA nuclease **(Fig 1E)**.
117 The second gene identified in our survey was *MYG1*, the yeast homolog of human MelanocYte
118 proliferation Gene 1, a 3'-5' RNA exonuclease associated with the human auto-immune disorder
119 vitiligo[38,39]. Phylogenetic analysis has identified *MYG1* orthologs across all taxa[38]. A *myg1*Δ *nuc1*Δ
120 double mutant strain displayed large increases of Gag accumulation compared to the single mutants and
121 exhibited L-A-dependent lethality at high temperature **(Fig S5A, S5B, and S5C)**. We were able to
122 recover *nuc1*Δ *ski3*Δ *myg1*Δ triple mutants, though they were extremely slow growing at 30˚ C and
123 accumulated even higher levels of Gag. These growth defects were also completely reversed in L-A$^0$
124 strains **(Fig S5C)**. *MYG1* thus represents a new viral attenuation factor, acting in parallel to both *NUC1*
125 and the *SKI* complex **(Fig 1E)**. Reflecting its underpinning as an auto-immune disease, Vitiligo is
126 associated with viral infection as well as with mutations in the intracellular viral sensor MDA5[40]. An
127 interesting possibility our findings suggest is that the elevated h*MYG1* expression associated with
128 vitiligo may reflect an antiviral role for this protein[39]. Indeed, growth defects caused by *myg1*Δ are
129 complemented by human Myg1, demonstrating a functional conservation to further investigate[38].
130 Although insightful studies of the L-A virus have been carried out, the L-A virus system has not
131 yet been extensively exploited as a model for studying innate antiviral immunity, owing largely to its
132 apparent benign nature. Here, we show that L-A is profoundly consequential for yeast fitness when its

133 replication is uncontrolled, and that diverse innate immune pathways contribute to maintaining L-A
134 replication at a harmless level. Importantly, our discovery that L-A is attenuated by homologs of known
135 human antiviral factors (*SRO9*/*SLF1* and *PAB1*) supports the hypothesis that *REX2* and *MYG1* homologs
136 may have viral innate immune functions in other organisms. Of note, Rex2 expands the arsenal of
137 mitochondrial localized antiviral nucleases beyond Nuc1, suggesting a key role of mitochondria in yeast
138 viral attenuation. Among the many possible explanations for this, one scenario is that some aspect of the
139 L-A replication cycle occurs in physical association with mitochondria similarly to as documented for
140 the plus strand ssRNA flock house virus[41]. Whatever the case may be, our results highlight a potential
141 general importance of mitochondria for viral innate immunity in eukaryotes, and position the yeast-L-A
142 system as a powerful model for further studies of this topic[42].
143
144 **Methods and Materials**
145
146 **Strains, media, and plasmids.**
147 Standard *S. cerevisiae* genetic and strain manipulation techniques were used for strain construction.
148 Refer to Table S1 for strains and plasmids used in this paper. The yOB255 *URA3::HSE-EmGFP* strain
149 was obtained from Onn Brandman[43]. The p5476 *2μ LEU2*, p5476 *NUC1 2μ LEU2*, p5476 *XRN1 2μ*
150 *LEU2*, p5476 *PAB1 2μ LEU2*, p5476 *SRO9 2μ LEU2*, p5476 *SLF1 2μ LEU2* MOBY plasmids were
151 obtained from Brenda Andrews[44]. The pVB3011 *L-BC GAG* ($P_{GAL1}$) plasmid was obtained from
152 Suzanne Sandmeyer[45].
153
154 **Spot analysis.**
155 Yeast strains were grown overnight at 30°C to saturation. Each strain was diluted to an $OD_{600}$ = 0.4,
156 serial diluted four times by 10-fold, and spotted onto agar plates containing synthetic complete media or
157 drop out media supplemented with the indicated carbon source (2% glucose or 3% glycerol).
158
159 **Protein extraction and Western blot.**
160 5 OD of log-phase cells were harvested and permeabilized with 0.1N NaOH at room temperature for 5
161 minutes. The cells were then pelleted and resuspended in SDS/PAGE buffer before heating at 100°C for
162 10 minutes. The samples were centrifuged to isolate the soluble fraction for Western blotting. Protein
163 concentrations were determined with an RC/DC assay (BioRad 5000121). Equal amounts of protein
164 were electrophoresed on 10% SDS/PAGE and transferred to poly(vinylidene difluoride) membranes.
165 Blots were incubated in primary antibody overnight and probed with 1:3,000 horseradish peroxidase

166 (HRP)-conjugated horse anti-mouse (7075; Cell Signaling Technology) or goat anti-rabbit (7074; Cell
167 Signaling Technology) secondary antibody. The proteins were detected with Luminata Forte Western
168 HRP Substrate (EMD Millipore) or SuperSignal™ West Atto Ultimate Sensitivity Substrate (A38555,
169 Thermo Scientific). Blots were imaged with the Bio-Rad ChemiDoc XRS+ system, and images were
170 processed with the Image Lab software package (Bio-Rad). The primary antibodies and their dilutions
171 were 1:5,000 anti-Pgk1 (ab113687; Abcam), 1:2,000 anti-L-A Gag (obtained from Reed Wickner),
172 1:8000 anti-Hsp60 (received from Toshiya Endo)[46], 1:500 anti-Tom22[46], 1:2000 anti-Om45[46]1:1000
173 anti-Cox2 (ab110271; Abcam), 1:1000 anti-Sro9, and 1:1000 anti-Slf1 (received from Sandra Wolin)[25].
174
175 **Virus curing.**
176 L-A$^0$ strains were generated similar to as we described previously[14]. Briefly, a progenitor L-A$^0$ strain
177 was isolated following treatment with 32 mM Anisomycin (BioShip ANS245) for 4 days in YPD media
178 and plating for single colonies. Isolates were tested for the presence of the L-A genome by RT-PCR.
179 This L-A$^0$ strain was then used for subsequent backcrossing with *mak3Δ* to generate other L-A$^0$ strain
180 background.
181
182 To evict L-BC, cells were transformed with the *L-BC GAG ($P_{GAL1}$)* plasmid and grown overnight in –
183 URA drop out media supplemented with 2% raffinose. The saturated culture was diluted and grown in
184 raffinose to log phase before treated with 2% galactose for 24 hours. The resulting culture was plated for
185 single colonies on an agar plate containing synthetic complete media supplemented with 5-FOA. Isolates
186 were tested for the presence of the L-BC genome by RT-PCR.
187
188 **RNA extraction and reverse transcription.**
189 10 OD of log phase cells was harvested and resuspended in phenol solution (P4682; Sigma-Aldrich),
190 SDS, and buffer AE (10 mM Tris·Cl and 0.5 mM EDTA, pH 9.0). Samples were incubated at 65°C for
191 30 minutes, and the phase-separated supernatant was washed with chloroform and precipitated in
192 isopropanol overnight. The precipitate was washed with 70% ethanol and dissolved in water. RNA
193 samples were then purified with the RNeasy Mini Kit (Qiagen). Four micrograms of RNA were reverse-
194 transcribed using random nonamers and Maxima H Minus Reverse Transcriptase (Thermo Fisher). The
195 cDNA product was isolated by alkaline hydrolysis and treated with RNase A.
196
197 **Immunofluorescence.**

198 Log phase cells were fixed with 4% formaldehyde and washed 2 times with 1x phosphate-buffered
199 saline (PBS). Cells were resuspended in sorbitol buffer (1.2 M sorbitol and 20 mM potassium phosphate
200 buffer, pH 7.2) and spheroplated with β-mercaptoethanol (M7522; Sigma-Aldrich) and zymolase at
201 30°C. Spheroplasted cells were added onto polylysine coated slides and incubated with primary antibody
202 1:1000 J2 anti-dsRNA (SCICONS) overnight. The cells were detected with 1:1000 cyanine3 conjugated
203 goat anti-mouse (Jackson ImmunoResearch Laboratories) and stained with DAPI. The images were
204 acquired with Zeiss Axio Imager Z1 and processed with ImageJ.
205
206 **Flow cytometry.**
207 Log phase cells were stained with propidium iodide, fixed with 4% formaldehyde, and washed 3 times
208 with 1x PBS. Fluorescence intensity was measured with Becton Dickinson LSR II flow cytometer and
209 analyzed with Flowing Software. The median GFP intensities of three biological replicates were plotted
210 using R ggplot2.
211
212 **High copy suppression screen.**
213 A plasmid library of random genomic inserts in the YEP24 plasmid backbone was transformed into a
214 *nuc1Δ ski3Δ* strain and spread onto -URA agar plate for single colonies[47]. Potential suppressors were
215 obtained by growing at 37°C supplemented with glycerol. To confirm that the suppression was plasmid
216 dependent, the potential suppressors were first grown on agar plate containing 0.1% 5-fluoroorotic acid
217 (5-FOA) for counterselection and then transferred to a fresh agar plate at 37°C supplemented with
218 glycerol. The plasmids of the candidates were isolated and sequenced to identify potential genes
219 responsible for the suppression of L-A pathogenesis when over-expressed. The candidate genes were
220 confirmed by spot analysis using p5476 MOBY plasmids.
221
222 **Acknowledgements**
223 We are grateful Dr. Charlie Boone and Dr. Brenda Andrews for generous sharing of strains and plasmid
224 and to Angus McQuibban for critical comments on the manuscript.
225
226
227
228 **References**
229

230 1. Bernheim, A., and Sorek, R. (2020). The pan-immune system of bacteria: antiviral defence as a
231 community resource. Nat Rev Microbiol *18*, 113-119. 10.1038/s41579-019-0278-2.
232 2. Wickner, R.B., Fujimura, T., and Esteban, R. (2013). Viruses and prions of Saccharomyces
233 cerevisiae. Adv Virus Res *86*, 1-36. 10.1016/B978-0-12-394315-6.00001-5.
234 3. Schmidt, N., Lareau, C.A., Keshishian, H., Ganskih, S., Schneider, C., Hennig, T., Melanson, R.,
235 Werner, S., Wei, Y., Zimmer, M., et al. (2021). The SARS-CoV-2 RNA-protein interactome in
236 infected human cells. Nat Microbiol *6*, 339-353. 10.1038/s41564-020-00846-z.
237 4. Smith, R.W., and Gray, N.K. (2010). Poly(A)-binding protein (PABP): a common viral target.
238 Biochem J *426*, 1-12. 10.1042/BJ20091571.
239 5. Brown, J.T., Bai, X., and Johnson, A.W. (2000). The yeast antiviral proteins Ski2p, Ski3p, and
240 Ski8p exist as a complex in vivo. RNA *6*, 449-457.
241 6. Benard, L., Carroll, K., Valle, R.C., Masison, D.C., and Wickner, R.B. (1999). The ski7 antiviral
242 protein is an EF1-alpha homolog that blocks expression of non-Poly(A) mRNA in
243 Saccharomyces cerevisiae. J Virol *73*, 2893-2900. 10.1128/JVI.73.4.2893-2900.1999.
244 7. Anderson, J.S., and Parker, R.P. (1998). The 3' to 5' degradation of yeast mRNAs is a general
245 mechanism for mRNA turnover that requires the SKI2 DEVH box protein and 3' to 5'
246 exonucleases of the exosome complex. EMBO J *17*, 1497-1506. 10.1093/emboj/17.5.1497.
247 8. Ball, S.G., Tirtiaux, C., and Wickner, R.B. (1984). Genetic Control of L-a and L-(Bc) Dsrna
248 Copy Number in Killer Systems of SACCHAROMYCES CEREVISIAE. Genetics *107*, 199-
249 217.
250 9. Rowley, P.A., Ho, B., Bushong, S., Johnson, A., and Sawyer, S.L. (2016). XRN1 Is a Species-
251 Specific Virus Restriction Factor in Yeasts. PLoS Pathog *12*, e1005890.
252 10.1371/journal.ppat.1005890.
253 10. Burgess, H.M., and Mohr, I. (2015). Cellular 5'-3' mRNA exonuclease Xrn1 controls double-
254 stranded RNA accumulation and anti-viral responses. Cell Host Microbe *17*, 332-344.
255 10.1016/j.chom.2015.02.003.
256 11. Ng, C.S., Kasumba, D.M., Fujita, T., and Luo, H. (2020). Spatio-temporal characterization of the
257 antiviral activity of the XRN1-DCP1/2 aggregation against cytoplasmic RNA viruses to prevent
258 cell death. Cell Death Differ *27*, 2363-2382. 10.1038/s41418-020-0509-0.
259 12. Eckard, S.C., Rice, G.I., Fabre, A., Badens, C., Gray, E.E., Hartley, J.L., Crow, Y.J., and Stetson,
260 D.B. (2014). The SKIV2L RNA exosome limits activation of the RIG-I-like receptors. Nat
261 Immunol *15*, 839-845. 10.1038/ni.2948.
262 13. Miyashita, M., Oshiumi, H., Matsumoto, M., and Seya, T. (2011). DDX60, a DEXD/H box
263 helicase, is a novel antiviral factor promoting RIG-I-like receptor-mediated signaling. Mol Cell
264 Biol *31*, 3802-3819. 10.1128/MCB.01368-10.
265 14. Gao, J., Chau, S., Chowdhury, F., Zhou, T., Hossain, S., McQuibban, G.A., and Meneghini,
266 M.D. (2019). Meiotic viral attenuation through an ancestral apoptotic pathway. Proc Natl Acad
267 Sci U S A *116*, 16454-16462. 10.1073/pnas.1900751116.
268 15. Li, L.Y., Luo, X., and Wang, X. (2001). Endonuclease G is an apoptotic DNase when released
269 from mitochondria. Nature *412*, 95-99. 10.1038/35083620.
270 16. Thomson, B.J. (2001). Viruses and apoptosis. Int J Exp Pathol *82*, 65-76. 10.1111/j.1365-
271 2613.2001.iep0082-0065-x.
272 17. Eastwood, M.D., Cheung, S.W., Lee, K.Y., Moffat, J., and Meneghini, M.D. (2012).
273 Developmentally programmed nuclear destruction during yeast gametogenesis. Dev Cell *23*, 35-
274 44. 10.1016/j.devcel.2012.05.005.
275 18. Eastwood, M.D., and Meneghini, M.D. (2015). Developmental Coordination of Gamete
276 Differentiation with Programmed Cell Death in Sporulating Yeast. Eukaryot Cell *14*, 858-867.
277 10.1128/EC.00068-15.

278 19. Koonin, E.V., and Krupovic, M. (2019). Origin of programmed cell death from antiviral
279 defense? Proc Natl Acad Sci U S A *116*, 16167-16169. 10.1073/pnas.1910303116.
280 20. Weber, F., Wagner, V., Rasmussen, S.B., Hartmann, R., and Paludan, S.R. (2006). Double-
281 stranded RNA is produced by positive-strand RNA viruses and DNA viruses but not in
282 detectable amounts by negative-strand RNA viruses. J Virol *80*, 5059-5064.
283 10.1128/JVI.80.10.5059-5064.2006.
284 21. Welsch, S., Miller, S., Romero-Brey, I., Merz, A., Bleck, C.K., Walther, P., Fuller, S.D., Antony,
285 C., Krijnse-Locker, J., and Bartenschlager, R. (2009). Composition and three-dimensional
286 architecture of the dengue virus replication and assembly sites. Cell Host Microbe *5*, 365-375.
287 10.1016/j.chom.2009.03.007.
288 22. Fernandez de Castro, I., Tenorio, R., and Risco, C. (2016). Virus assembly factories in a lipid
289 world. Curr Opin Virol *18*, 20-26. 10.1016/j.coviro.2016.02.009.
290 23. Liu, Y.X., and Dieckmann, C.L. (1989). Overproduction of yeast viruslike particles by strains
291 deficient in a mitochondrial nuclease. Mol Cell Biol *9*, 3323-3331.
292 24. Johnson, A.W., and Kolodner, R.D. (1995). Synthetic lethality of sep1 (xrn1) ski2 and sep1
293 (xrn1) ski3 mutants of Saccharomyces cerevisiae is independent of killer virus and suggests a
294 general role for these genes in translation control. Mol Cell Biol *15*, 2719-2727.
295 25. Sobel, S.G., and Wolin, S.L. (1999). Two yeast La motif-containing proteins are RNA-binding
296 proteins that associate with polyribosomes. Mol Biol Cell *10*, 3849-3862.
297 10.1091/mbc.10.11.3849.
298 26. Proweller, A., and Butler, J.S. (1996). Ribosomal association of poly(A)-binding protein in
299 poly(A)-deficient Saccharomyces cerevisiae. J Biol Chem *271*, 10859-10865.
300 10.1074/jbc.271.18.10859.
301 27. Brandman, O., Stewart-Ornstein, J., Wong, D., Larson, A., Williams, C.C., Li, G.W., Zhou, S.,
302 King, D., Shen, P.S., Weibezahn, J., et al. (2012). A ribosome-bound quality control complex
303 triggers degradation of nascent peptides and signals translation stress. Cell *151*, 1042-1054.
304 10.1016/j.cell.2012.10.044.
305 28. Anckar, J., and Sistonen, L. (2011). Regulation of HSF1 function in the heat stress response:
306 implications in aging and disease. Annu Rev Biochem *80*, 1089-1115. 10.1146/annurev-
307 biochem-060809-095203.
308 29. Sorger, P.K., and Pelham, H.R. (1987). Purification and characterization of a heat-shock element
309 binding protein from yeast. EMBO J *6*, 3035-3041.
310 30. Li, J., Labbadia, J., and Morimoto, R.I. (2017). Rethinking HSF1 in Stress, Development, and
311 Organismal Health. Trends Cell Biol *27*, 895-905. 10.1016/j.tcb.2017.08.002.
312 31. Stark, C., Breitkreutz, B.J., Reguly, T., Boucher, L., Breitkreutz, A., and Tyers, M. (2006).
313 BioGRID: a general repository for interaction datasets. Nucleic Acids Res *34*, D535-539.
314 10.1093/nar/gkj109.
315 32. Koonin, E.V. (1997). A conserved ancient domain joins the growing superfamily of 3'-5'
316 exonucleases. Curr Biol *7*, R604-606. 10.1016/s0960-9822(06)00311-3.
317 33. Espert, L., Degols, G., Gongora, C., Blondel, D., Williams, B.R., Silverman, R.H., and Mechti,
318 N. (2003). ISG20, a new interferon-induced RNase specific for single-stranded RNA, defines an
319 alternative antiviral pathway against RNA genomic viruses. J Biol Chem *278*, 16151-16158.
320 10.1074/jbc.M209628200.
321 34. Zuo, Y., and Deutscher, M.P. (2001). Exoribonuclease superfamilies: structural analysis and
322 phylogenetic distribution. Nucleic Acids Res *29*, 1017-1026. 10.1093/nar/29.5.1017.
323 35. Hanekamp, T., and Thorsness, P.E. (1999). YNT20, a bypass suppressor of yme1 yme2, encodes
324 a putative 3'-5' exonuclease localized in mitochondria of Saccharomyces cerevisiae. Curr Genet
325 *34*, 438-448. 10.1007/s002940050418.

326 36. van Hoof, A., Lennertz, P., and Parker, R. (2000). Three conserved members of the RNase D
327 family have unique and overlapping functions in the processing of 5S, 5.8S, U4, U5, RNase
328 MRP and RNase P RNAs in yeast. EMBO J *19*, 1357-1365. 10.1093/emboj/19.6.1357.
329 37. Szewczyk, M., Malik, D., Borowski, L.S., Czarnomska, S.D., Kotrys, A.V., Klosowska-Kosicka,
330 K., Nowotny, M., and Szczesny, R.J. (2020). Human REXO2 controls short mitochondrial RNAs
331 generated by mtRNA processing and decay machinery to prevent accumulation of double-
332 stranded RNA. Nucleic Acids Res *48*, 5572-5590. 10.1093/nar/gkaa302.
333 38. Grover, R., Burse, S.A., Shankrit, S., Aggarwal, A., Kirty, K., Narta, K., Srivastav, R., Ray,
334 A.K., Malik, G., Vats, A., et al. (2019). Myg1 exonuclease couples the nuclear and mitochondrial
335 translational programs through RNA processing. Nucleic Acids Res *47*, 5852-5866.
336 10.1093/nar/gkz371.
337 39. Dwivedi, M., Laddha, N.C., and Begum, R. (2013). Correlation of increased MYG1 expression
338 and its promoter polymorphism with disease progression and higher susceptibility in vitiligo
339 patients. J Dermatol Sci *71*, 195-202. 10.1016/j.jdermsci.2013.04.026.
340 40. Zhuang, T., Yi, X., Chen, J., Kang, P., Chen, X., Chen, J., Cui, T., Chang, Y., Ye, Z., Ni, Q., et
341 al. (2020). Intracellular virus sensor MDA5 exacerbates vitiligo by inducing the secretion of
342 chemokines in keratinocytes under virus invasion. Cell Death Dis *11*, 453. 10.1038/s41419-020-
343 2665-z.
344 41. Kopek, B.G., Perkins, G., Miller, D.J., Ellisman, M.H., and Ahlquist, P. (2007). Three-
345 dimensional analysis of a viral RNA replication complex reveals a virus-induced mini-organelle.
346 PLoS Biol *5*, e220. 10.1371/journal.pbio.0050220.
347 42. West, A.P., Shadel, G.S., and Ghosh, S. (2011). Mitochondria in innate immune responses. Nat
348 Rev Immunol *11*, 389-402. 10.1038/nri2975.
349 43. Sitron, C.S., Park, J.H., Giafaglione, J.M., and Brandman, O. (2020). Aggregation of CAT tails
350 blocks their degradation and causes proteotoxicity in S. cerevisiae. PLoS One *15*, e0227841.
351 10.1371/journal.pone.0227841.
352 44. Magtanong, L., Ho, C.H., Barker, S.L., Jiao, W., Baryshnikova, A., Bahr, S., Smith, A.M.,
353 Heisler, L.E., Choy, J.S., Kuzmin, E., et al. (2011). Dosage suppression genetic interaction
354 networks enhance functional wiring diagrams of the cell. Nat Biotechnol *29*, 505-511.
355 10.1038/nbt.1855.
356 45. Bilanchone, V., Clemens, K., Kaake, R., Dawson, A.R., Matheos, D., Nagashima, K., Sitlani, P.,
357 Patterson, K., Chang, I., Huang, L., and Sandmeyer, S. (2015). Ty3 Retrotransposon Hijacks
358 Mating Yeast RNA Processing Bodies to Infect New Genomes. PLoS Genet *11*, e1005528.
359 10.1371/journal.pgen.1005528.
360 46. Sakaue, H., Shiota, T., Ishizaka, N., Kawano, S., Tamura, Y., Tan, K.S., Imai, K., Motono, C.,
361 Hirokawa, T., Taki, K., et al. (2019). Porin Associates with Tom22 to Regulate the
362 Mitochondrial Protein Gate Assembly. Mol Cell *73*, 1044-1055 e1048.
363 10.1016/j.molcel.2019.01.003.
364 47. Kamada, Y., Fujioka, Y., Suzuki, N.N., Inagaki, F., Wullschleger, S., Loewith, R., Hall, M.N.,
365 and Ohsumi, Y. (2005). Tor2 directly phosphorylates the AGC kinase Ypk2 to regulate actin
366 polarization. Mol Cell Biol *25*, 7239-7248. 10.1128/MCB.25.16.7239-7248.2005.
367

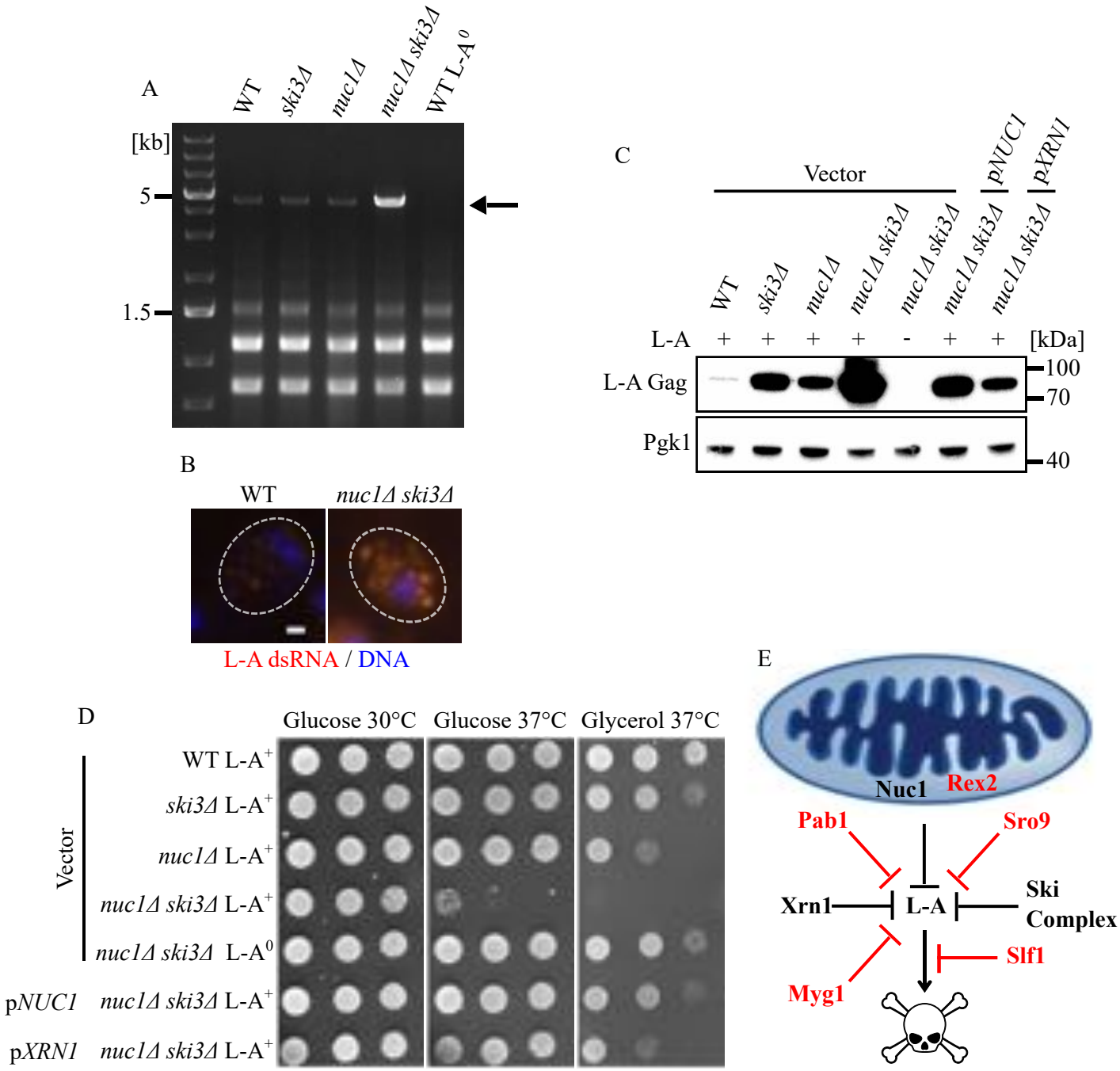


**Figure 1**. L-A attenuation protects yeast from lethal pathogenesis. **(A)** An ethidium bromide-stained gel of total RNA prepared from the indicated strains is shown, with the 4.6 Kb L-A dsRNA band indicated with an arrow. **(B)** Immunofluorescence was used to visualize L-A dsRNA (red) in cells of the indicated genotypes. These strains were cured of the weakly abundant L-BC dsRNA virus to eliminate background staining (see Methods). DAPI staining of DNA is shown in blue. Scale bar, 1 µm. **(C)** Western blotting of L-A Gag and Pgk1 protein levels in the indicated strains is shown. Molecular weight markers are indicated on the right. **(D)** Spot test growth assays of the strains from 1C is shown. Strains were spotted on -Leu media containing either glucose or glycerol and grown at the indicated temperatures. **(E)** The mitochondrial proteins Nuc1 and Rex2 collaborate with the cytosolic proteins Xrn1, SkiC, and Myg1 to regulate L-A protein level and ensure cell fitness. The translation control factors Pab1 and Sro9 alleviate L-A pathogenesis by suppressing L-A level while Slf1, the paralog of Sro9, suppress L-A pathogenesis without affecting L-A level. Newly discovered L-A attenuation factors are indicated in red.

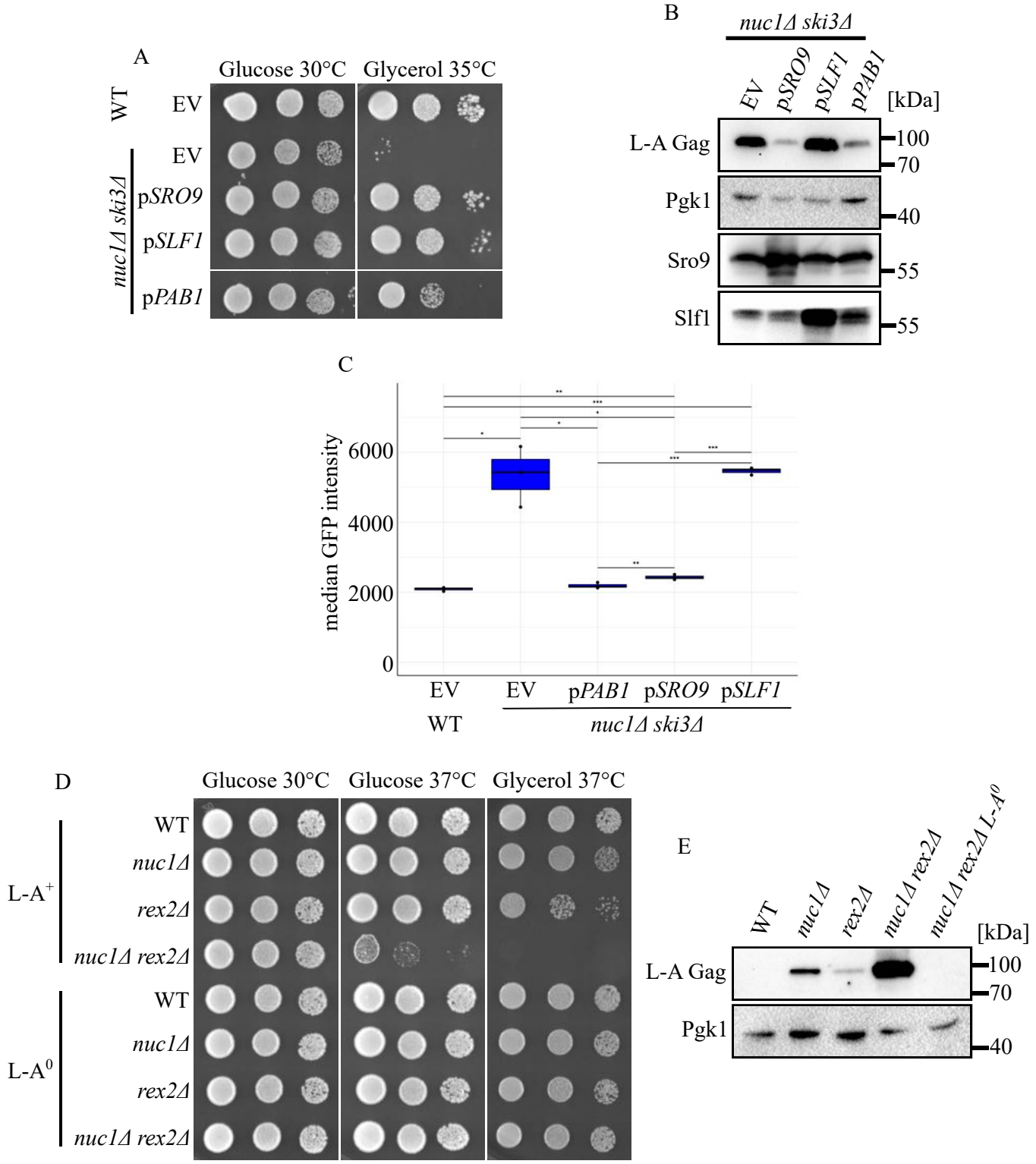


**Figure 2**. New antiviral factors are identified by exploiting the L-A pathogenesis. **(A)** Spot test growth assays of the high copy suppressors *SRO9*, *SLF1*, and *PAB1* are shown. **(B)** Western blotting detection of L-A Gag, Pgk1, Sro9, and Slf1 protein levels in the strains from 2A is shown. Molecular weight markers are indicated on the right. **(C)** Flow cytometry was used to measure HSE-GFP expression in the indicated strains. Median GFP intensity is shown. n = 3. * $p < 0.05$, ** $p < 0.01$, *** $p < 0.001$. The $p$ value was calculated using the unpaired student's t-test. **(D)** Spot analysis of strains defective in *NUC1* and *REX2* is shown. Strains are spotted on SC media containing either glucose or glycerol and grown at the indicated temperature. **(E)** Western blotting of L-A Gag and Pgk1 protein levels of strains in Figure 2D. Molecular weight markers are indicated on the right.

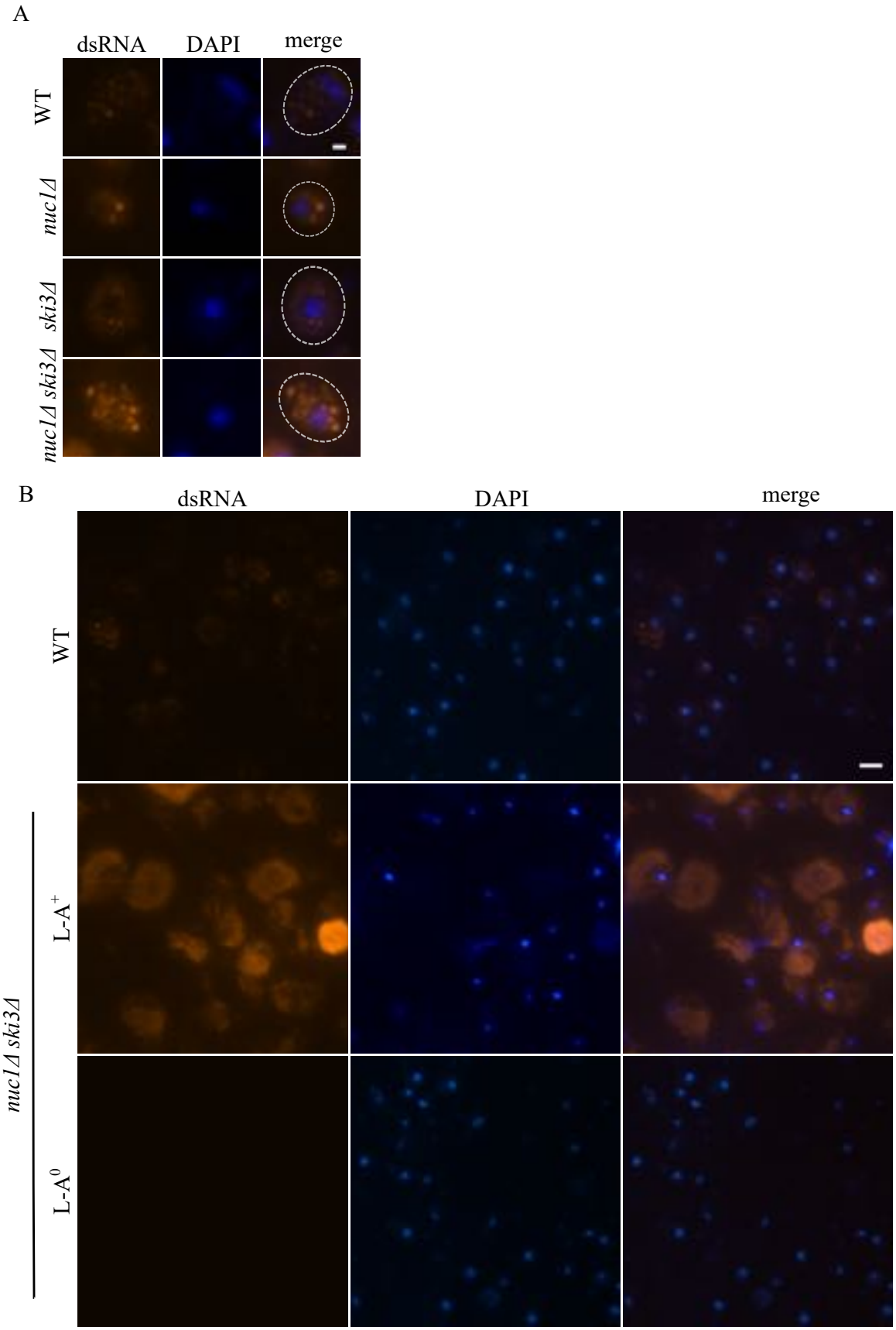


**Figure S1**. Additional images of immunofluorescence of dsRNA (red) of strains from Figure 1B. **(A)** Immunofluorescence of dsRNA (red) of indicated genotype is shown. Cells are stained with DAPI to visualize nuclei. Scale bar, 1 µm. **(B)** Images of fields of cells of indicated genotype is shown. Cells are stained with DAPI to visualize nuclei. Scale bar, 30 µm.

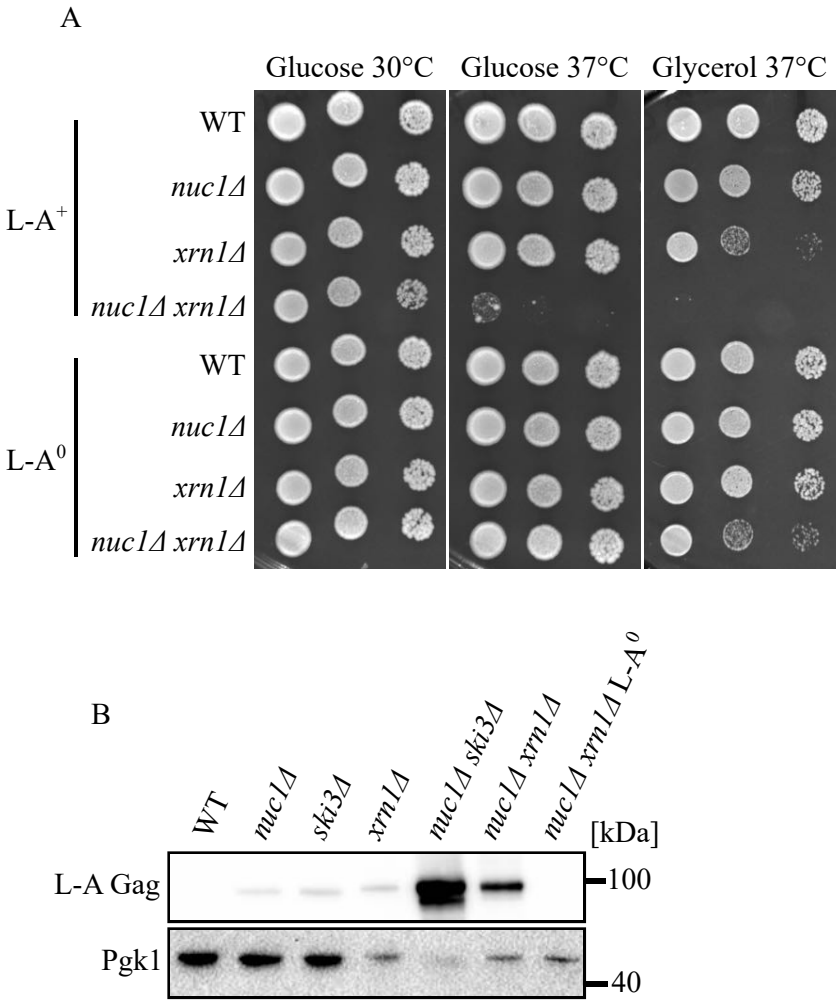


**Figure S2**. *XRN1*, *NUC1*, and *SKI3* work in parallel pathways to regulate L-A Gag level. **(A)** Spot analysis of strains defective in *NUC1* and *XRN1* is shown. Strains are spotted on SC media containing either glucose or glycerol and grown at the indicated temperature. **(B)** Western blotting of L-A Gag and Pgk1 protein levels of strains in Figure S2A. Molecular weight markers are indicated on the right.

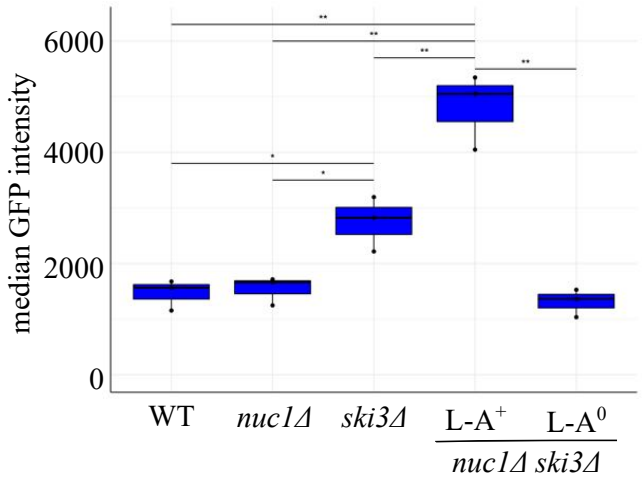


**Figure S3**. L-A pathogenesis correlates with proteostatic stress. Flow cytometry was used to measure HSE-GFP expression in the indicated strains. Median GFP intensity is shown. n = 3. * $p < 0.05$, ** $p < 0.01$. The $p$ value was calculated using unpaired student's t-test.

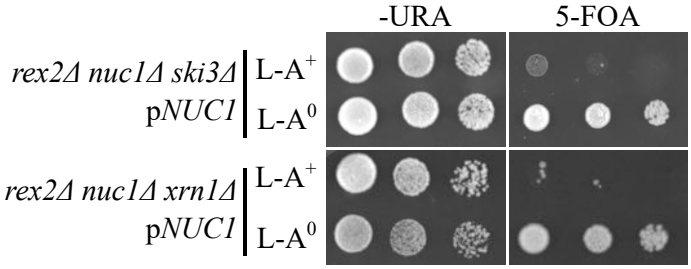


**Figure S4**. The mitochondrial exonuclease *REX2* is an antiviral factor. Spot analysis of strains defective in 3 parallel antiviral pathways containing plasmid expressing *NUC1* is shown. Strains are spotted on -URA media or synthetic complete (SC) media supplemented with 0.1% 5-fluoroorotic acid (5-FOA).

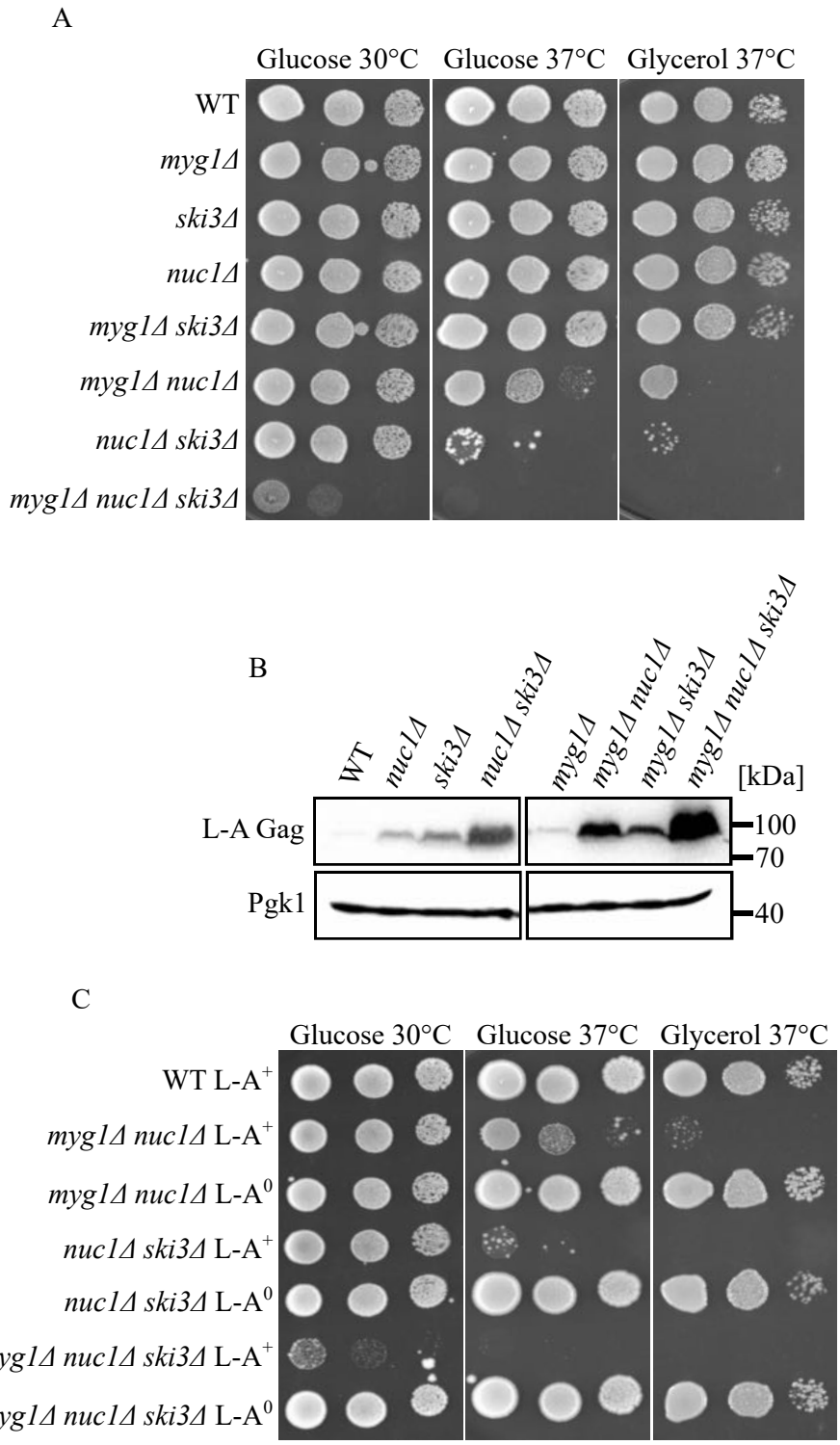


**Figure S5**. *MYG1* collaborates with *NUC1* and *SKI3* to ensure cell fitness in a L-A dependent manner. **(A)** Spot analysis of strains defective in *MYG1*, *NUC1*, and *SKI3* is shown. Strains are spotted on SC media containing either glucose or glycerol and grown at the indicated temperature. **(B)** Western blotting detection of L-A Gag and Pgk1 protein levels in the indicated strains is shown. Molecular weight markers are indicated on the right. **(C)** Spot analysis of strains defective in *MYG1*, *NUC1*, and *SKI3* with and without L-A is shown. Strains are spotted on SC media containing either glucose or glycerol and grown at the indicated temperature.